A&A 421, 821–832 (2004)
DOI: 10.1051/0004-6361:20035842

Astronomy & Astrophysics

Number counts of bright extremely red objects: Evolved massive galaxies at $z \sim 1$

P. Väisänen[1,2] and P. H. Johansson[3,4]

[1] European Southern Observatory, Alonso de Cordova 3107, Casilla 19001, Santiago, Chile
[2] Departamento de Astronomía, Universidad de Chile, Casilla 36-D, Santiago, Chile
[3] Institute of Astronomy, Madingley Road, Cambridge, CB3 0HA, UK
[4] Observatory, PO Box 14, 00014 University of Helsinki, Finland

Received 10 December 2003 / Accepted 8 April 2004

Abstract. We present results on number counts of Extremely Red Objects (EROs) in a 2850 arcmin^2 near-infrared survey performed in European Large Area ISO Survey (ELAIS) fields at $K < 17.5$. Counts of EROs are extended to brighter levels than available previously, giving 0.002 ± 0.001 arcmin^{-2} at $K < 16.5$ and consistent numbers with literature values at fainter magnitudes. Photometric redshifts from HYPERZ as well as GRASIL model SEDs of galaxies imply that our EROs are located in the range $z = 0.7-1.5$, with the bulk of the population at $z \sim 1$. Taking advantage of the ISO data in the fields, we use mid-IR detections to constrain the number of dusty EROs, and also discuss the superior capabilities of Spitzer Space Telescope to detect dusty EROs. Both the mid-IR data and the use of colour−colour diagrammes indicate that at most 10−20% of the EROs in this bright regime are dusty starbursting systems. The space density of our EROs, interpreted to be counterparts of local $>2-3$ $L^\star$ massive galaxies at around $z \sim 1$, is estimated to be $\approx 2 \times 10^{-5}$ Mpc^{-3}, which is consistent with local values. Furthermore, the cumulative number counts at our bright magnitudes are remarkably well fitted by pure luminosity evolution models.

Key words. galaxies: evolution – galaxies: formation – infrared: galaxies – cosmology: observations – galaxies: starburst – galaxies: elliptical and lenticular, cD

1. Introduction

Extremely Red Objects (EROs, selected for example by $R - K > 5$, $I - K > 4$ colours) have received much focus recently by virtue of their potential as a powerful window into the galaxy formation era. By and large, the majority of EROs have been incorporated into a bimodal population, where the extreme red colours are attributed either to old passively evolving distant ($z > 1$) elliptical galaxies or to extremely dust reddened starburst galaxies (see e.g. recent papers by Cimatti et al. 2003; Wold et al. 2003; Yan & Thompson 2003; Takata et al. 2003; Daddi et al. 2002; Smail et al. 2002; Roche et al. 2002, and references therein for earlier pioneering ERO surveys). It is the class of aged early type galaxies whose number densities provide the strongest constraints on models of galaxy evolution. On the other hand, the dusty EROs could be related to the (ultra) luminous IR-galaxies producing the bulk of the total energy in the Universe since the recombination era (see e.g. Elbaz & Cesarsky 2003 for a review).

The dusty ERO population contaminates the otherwise, in principle, clean samples of high redshift massive ellipticals. This is the reason why the separation of elliptical EROs from dusty EROs, using photometric, spectroscopic, and morphological analyses, has received the main attention of ERO studies recently. In general, a large number of massive galaxies at redshifts of unity and over would support a traditional monolithic collapse scenario where galaxies form at high redshift in a single collapse and then evolve passively (e.g. Eggen et al. 1962; Larson 1975). Significantly smaller numbers of massive high-z ellipticals on the other hand fit predictions from the hierarchical assembly scenarios, where massive galaxies are formed only relatively recently from the merging of smaller units (e.g., White & Rees 1978; White & Frenk 1991; Somerville & Primack 1999; Cole et al. 2000).

Since EROs are extremely faint optically ($R \geq 24$), their redshifts and spectral and morphological properties have remained largely unknown until very recently. Cimatti et al. (2002) carried out a VLT spectroscopic survey of 45 EROs with $R - K > 5$ and $K_s < 19.2$. They identified approximately 1/3 of the EROs as old elliptical systems, 1/3 as dusty starburst galaxies, while 1/3 remained unidentified. The mean redshift was found to be $z \sim 1.0$ for both populations. Yan et al. (2004) on the other hand find a small 10−15% fraction of isolated passive systems. Yan & Thompson (2003), Cimatti et al. (2003), Moustakas et al. (2004), and Gilbank et al. (2003) have used HST morphologies to differentiate between the classes: the

Send offprint requests to: P. Väisänen,
e-mail: pvaisane@eso.org

results have further complicated the picture, as a large fraction (25−65%) of EROs seem to be disks (though see also Moriondo et al. 2000). The expectation originally had been a clearer distinction into spheroids on one side, and irregular and interacting types on the other, expected for extremely dusty star forming galaxies. The relative fractions of different types of EROs thus still remain uncertain (due to for example different selection criteria used) and the results of testing surface densities against galaxy formation scenarios are inconclusive.

In addition to spectroscopic and morphological methods mentioned above, one may separate the old elliptical and dusty EROs by means of longer wavelength observations: any ERO detected at mid-IR to radio wavelengths should belong to the dusty population. Systematically this has been attempted by Mohan et al. (2002) in the sub-mm to radio and Smail et al. (2002) in the radio. Similar fractions (albeit with wide spread) as referred to above of dusty EROs were found in the latter study, while Mohan et al. (2002) find a much lower fraction.

In this paper we attempt to separate EROs, for the first time, based on their mid-IR properties. As with far-IR to radio methods, this is a clear-cut definition, since the difference of ellipticals and starbursting galaxies is very large – distant evolved ellipticals would not be detected with ISO whereas dusty EROs should have strong mid-IR flux. Also, mid-IR avoids the identification problems of e.g. large sub-mm beams. We have surveyed an ISO/ELAIS (European Large Area *ISO* Survey; Oliver et al. 2000) field in the near-IR and matched the results with an optical dataset. We make use of the newly available Final ELAIS Catalogue (Rowan-Robinson et al. 2004). In this paper we consider the surface densities of EROs resulting from a wide-field relatively shallow J and K-band survey. We shall present the results from a deeper NIR survey around faint mid-IR detections in subsequent papers (Väisänen & Johansson 2004; Johansson et al. 2004, in prep.).

The structure of this paper is as follows. The observational data are presented in Sect. 2, and in Sect. 3 we define and extract the ERO sample from the photometric catalogues. In Sect. 4 we discuss the dusty vs. evolved ERO separation and in Sect. 5 the SEDs of the detected EROs. The resulting surface densities of EROs are presented in Sect. 6. We assume throughout this paper a flat ($\Omega_0 = 1$) cosmology with $\Omega_\mathrm{m} = 0.3$, $\Omega_\Lambda = 0.7$ and $H_0 = 70\ \mathrm{km\,s^{-1}\ Mpc^{-1}}$.

2. Observations

2.1. Near-infrared data

The observations presented here were conducted in the ELAIS fields N1 and N2, centered at $(\alpha, \delta) = 16\mathrm{h}09\mathrm{m}00\mathrm{s}, 54°40'00''$ and $(\alpha, \delta) = 16\mathrm{h}36\mathrm{m}00\mathrm{s}, 41°06'00''$ J2000.0 respectively.

The near-IR survey performed with the Mt.Hopkins 1.2-m telescope, reaching limiting magnitudes of approximately $J = 19.3$ and $K = 17.5$, is fully presented in Väisänen et al. (2000, hereafter V00). The data cover a total of one square degree, although a slightly smaller area is used here (2850 arcmin^2) after some edges and higher noise areas were excluded and, more importantly, only areas with full coverage in both bands were considered. The detector used was a 256×256 InSb array with $1.2''$ pixels.

2.2. Optical data

We obtained optical photometric data from the Isaac Newton Telescope (INT) Wide Field Survey (WFS). The WFS data are publicly available on the Cambridge Astronomical Survey Unit (CASU) homepage[1]. For a review on the INT Wide Field Survey Project and instrument characteristics, see McMahon et al. (2001). The data consist of U, g', r', i', Z band photometry (Vega-based) in the N1 region and g', r', i', Z photometry in the N2 region (the apostrophes are dropped henceforward for clarity). The WFS bandpasses are similar to the SDSS (Sloan Digital Sky Survey) filters (Fukugita et al. 1996). The WFS webpage[2] gives colour transformations between the WFS filters and those of the standard Johnson-Cousins system (Landolt 1992): $r - R = 0.275(R - I) + 0.008$ and $i - I = +0.211(R - I)$ for the bands most used in this paper. The nominal 5σ detection limits for a $1''$ seeing are $g \approx 25.0$, $r \approx 24.1$, $i \approx 23.2$, and $Z \approx 22.0$ (the WFS page). For further details on the pipeline processing of INT wide field survey data consult Irwin & Lewis (2001), and Gonzalez-Solares et al. (2004) for more in-depth discussion of the WFS data in particular in ELAIS fields. We also obtained raw R-band images of the ELAIS N1 and N2 regions from the archives. After reduction we used them for object identification – only the pipeline processed catalogues were used for photometry however.

2.3. Astrometry and photometry

The INT astrometry was derived using Guide Star Catalog (GSC) stars, which results in an external astrometric accuracy of $0.5''-1.0''$ (Irwin & Lewis 2001). Astrometric accuracy in the Mt.Hopkins data ranges between $0.5-1.5''$, and was calibrated using GSC and US Naval Observatory (USNO) catalogues.

All our near-IR photometry is performed using the SExtractor software (v.2.2.1 and v.2.3; Bertin & Arnouts 1996). Our NIR photometry is explained in V00. As discussed therein, we used total magnitudes as given by the SExtractor "BEST"-magnitude. However, since the optical WFS photometry was given only in $2.4''$ diameter aperture magnitudes, we re-did all the old photometry with matching apertures. It is crucial that the different observations map the same region of the source when constructing colour indices; near-IR magnitudes *not* associated with colours are given as total magnitudes in this paper.

The archive optical INT WFS data in the ELAIS regions come as fully calibrated photometric source catalogues (Irwin & Lewis 2001; Gonzalez-Solares et al. 2004). No further processing is done for the catalogue except merging of multiple and/or nearby sources, as described below in Sect. 3.2.

[1] http://archive.ast.cam.ac.uk/

[2] http://www.ast.cam.ac.uk/~wfcsur/index.php

3. Construction of the ERO samples

3.1. Definition of EROs

Numerous different selection criteria have been defined for EROs, including $R-K \geq 6$, $R-K \geq 5.3$, $R-K \geq 5$, $I-K \geq 4$ with K-magnitude upper limits from 18 to 21 mag. All these criteria are designed for selecting early type galaxies at $z \geq 1$. In this paper we use the following definition for EROs: $r-K \geq 5.5$ and/or $i-K \geq 4.4$. Our limits result from colour transformations given above in Sect. 2.2 for typical colours of $R-I \approx 1.4-2.0$ of our sources, and from the desire to have limits corresponding to the commonly used $R-K > 5$, $I-K > 4$ selections to aid comparisons to other surveys. In addition, we will check any results with $r-K > 5.8$, i.e. $R-K \geq 5.3$, which is also often used.

Furthermore, we calculated $r-R$ and $i-I$ colours using SEDs from the GRASIL library (Silva et al. 1998) and verified the $r-R \approx 0.5$ and $i-I \approx 0.4$ colours to match well those of ellipticals at $z \sim 1$. Naturally an exact comparison or transformation between different galaxy colour selection criteria is redshift and galaxy SED dependent, and we note that since the model colours that different authors use vary, there might easily be 0.1−0.3 mag differences in the colours at $z \sim 1$. Elliptical galaxies become EROs at $z \approx 1.1-1.2$ with the criteria and models we used.

Figure 1 shows $r-K$ and $i-K$ model colours of several representative galaxies against redshift with the ERO criteria included. Model SEDs are adopted from the GRASIL library (Silva et al. 1998; model SEDs and the GRASIL code are available online[3]). Ordinary spirals (dotted line) never reach the red colours of EROs, while both ellipticals (solid) and reddened starbursts (dash-dot) become EROs when seen beyond $z \sim 1$. For comparison, the colour of the prototype dusty ERO HR10 is also plotted (dashed curve) as a function of redshift. The colour of the HR10 model is due to extreme dust extinction (Silva 1999). The lowest panel shows the flux ratio $f_{15\,\mu\mathrm{m}}/f_{2.2\,\mu\mathrm{m}}$ – the degeneracy in the red colours of old ellipticals and dusty starbursts is clearly broken, as will be discussed later in more detail.

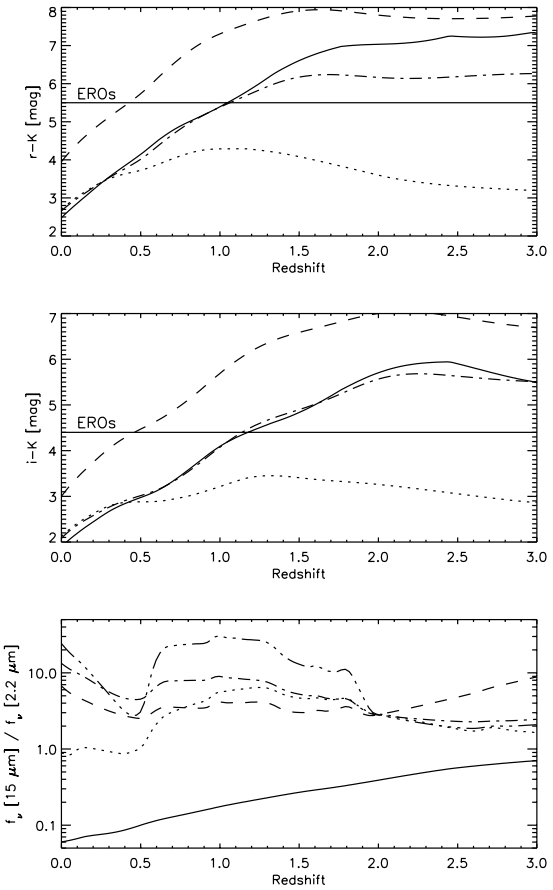

Fig. 1. Observed $r-K$ and $i-K$ and MIR/NIR colours of representative galaxies are calculated from model SEDs of GRASIL code (Silva et al. 1998). An evolving Sb spiral (dotted line) is plotted along with an evolving elliptical (solid curve). Non-evolving models fitted to the observed rest-frame SEDs of the prototypical starburst M 82 (dash-dot) and HR10 ERO (dashed), are also plotted. Solid horizontal lines show the colour definition of EROs in this paper. The dash-triple-dot curve in the lowest panel corresponds to the ULIRG Arp220, which gives the most extreme MIR/NIR colours.

3.2. Matching of optical and NIR data

The optical counterparts of near-IR sources in the J and K-band matched Mt.Hopkins catalogue were extracted from the INT WFS catalogue using 3″ search radius. More than 80% of the matches are found within ≈1.5″ separations, which is reasonable given the astrometric accuracies and pixel sizes. Approximately 4% of the 6600 NIR sources in the Mt.Hopkins catalogue were not matched with an optical source. We checked these individually: the great majority are close to WFS CCD edges or bright stars, or were some remaining NIR frame cosmic rays, etc., and though a handful of these may be genuine very red objects (though not necessarily EROs) we decided to conservatively exclude all of these from the final source list.

[3] http://web.pd.astro.it/granato/

Since the WFS catalogue contains multiple detections of the same source (due to overlapping CCD frames), optical counterparts within 0.5″ of each other were averaged. After this purging, the remaining multiple matches within 1.5″ were summed up since the corresponding NIR catalogue would not have resolved them as individual sources, and then the brightest source was selected if there still were multiple counterparts available. Approximately 18% of the original WFS optical catalogue closest matches were affected by the purging, though less than 4% by more than 0.1 mag.

3.3. Star vs. galaxy separation

We then proceeded to separating stars from galaxies in the surveys. Stellarity indices were available from both the NIR catalogue (the SExtractor CLASS parameter) and the WFS catalogue, where a flag defines galaxies, definite stars, and various degrees of uncertain stellarities. The WFS classification is in principle more useful for us here, since it goes deeper than the NIR data. Note that the star-galaxy separation is different from

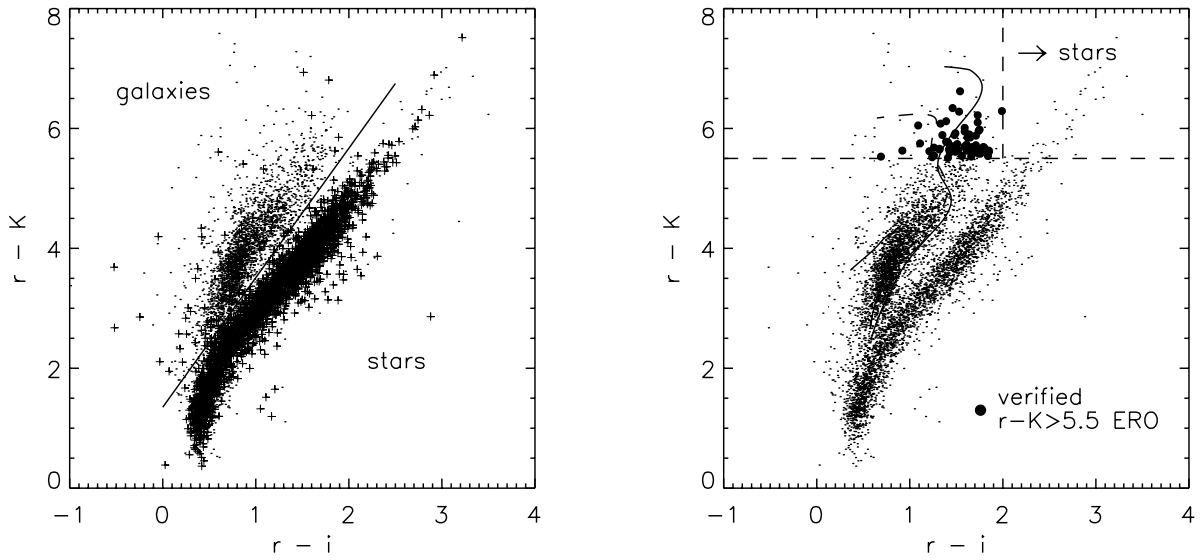

Fig. 2. Observed $r - i$ vs. $r - K$ colours of our survey. Stellar sources, as defined by the WFS classification are overplotted as small crosses in the left panel. It is seen that this colour−colour diagramme does a very good job in separating stars from galaxies: in particular there is virtually no overlap in the region of interest, at $r - K > 5$. Any "ERO" with $r - i > 2$ is classified as a star. The right panel shows all the galaxy EROs of the Mt.Hopkins survey selected with $r - K > 5.5$ and several GRASIL model SEDs overplotted: the lowest solid curve is the SED of an Sb galaxy, the dashed curve reaching ERO regime is that of a starburst, and the highest curve an elliptical. The curves are plotted up to redshift of $z = 2$ (see text and Sect. 3.1).

that conducted in V00 since we now have a much deeper optical catalogue available.

However, for the EROs we are interested in, the reddest and faintest objects in the catalogue, we find that a colour separation works best. This can be seen in Fig. 2, which shows the full catalogue in $r - i$ vs. $r - K$ with the morphological classification indicated: stars are overplotted as small crosses in the left panel. A separating line, adjusted experimentally to maximally distinguish the main concentrations of stellar and extended sources in the figure, of $r - K = 2.16(r - i) + 1.35$ is drawn. This colour−colour diagramme separates stars very well from galaxies; it is important to note that there is virtually no overlap between the stellar sources and galaxies in the region of interest at $r - K > 5$. The $r - i$ colour, in fact, is very important in the separation of red stars. Very low mass and cool stars (of the L spectral type in particular) have $R - K$ and $J - K$ colours closely mimicking those of extragalactic EROs – for these stars, however, $R - I$ (or $r - i$) always stays above ≈ 2 (see e.g. Chabrier et al. 2000; Cruz et al. 2003). On the other hand, we find no galaxy models resulting in $r - i > 2$ colours (GRASIL code used; see also e.g. Fugukita et al. 1995). All extremely red objects with $r - i > 2$ can safely be discarded as stars.

Representative galaxy colours calculated from GRASIL models (Silva et al. 1998) are overplotted in the right panel. In fact, the elliptical model does overlap with the $r - i \sim 3$ extremely red stars, but only at $z > 4$. This is a potential concern with deeper ERO surveys, but at our brighter magnitudes such distant sources are not expected to be seen.

We thus use a combination of methods. We define as stellar all objects having stellar colours according to the above limit *and* those *not* having a galaxy morphology set by the WFS survey. The end result of this is that brighter sources are preferentially separated by morphology and fainter ones (especially red sources) by colour. The star counts were already compared to the SKY model predictions of Cohen (1994) in V00, and found to fit well model predictions for the corresponding fields. In the regime $K < 17.5$, 45% of $r - K > 5.5$ sources were classified as stars. In summary, it should be stressed that in the case of bright surveys of EROs, the contamination from red late type (typically L-type) stars is considerable when using the $R - K$ based selections of EROs.

3.4. Extraction of EROs

We searched for EROs from the Mt.Hopkins galaxy catalogue according to the colour definitions given above in Sect. 3.1. Only NIR detections at 5σ level and over were considered. We then went through the resulting list checking our NIR maps as well as the WFS CCD images for any obvious spurious objects (for example, anomalously low optical magnitudes were found in cases when sources fell close to gaps in the CCD frames, or near bright stars – these were excluded). Ultimately there were 50 EROs in the matched Mt.Hopkins catalogue using the $r - K$ criterion and 21 using the $i - K$ limit – 17 EROs are common to lists resulting from both selection criteria. This makes 54 EROs in total. All the EROs have an i-band detection, while there were 4 EROs which have only upper limits in the r-band. It is obvious that the r and i band based selection criteria for EROs are not equivalent. There are more than twice as much $r - K > 5.5$ selected EROs than $i - K > 4.4$ selected ones.

The photometry for all EROs is given in Table 1 and the resulting total numbers of verified EROs are summarized in Table 2, along with some other survey characteristics. The colour−magnitude plot is shown in Fig. 3.

Table 1. Photometry of the whole ERO sample. Sources 1–17 are those with $r - K > 5.5$ and $i - K > 4.4$, while 18–50 and 51–54 are selected by only $r - K > 5.5$ and $i - K < 4.4$, respectively.

	RA (J2000)	Dec (J2000)	g'	r'	i'	Z	J	K
1	$16^h08^m57.0^s$	54°43′12.2″	24.34 ± 0.12	23.62 ± 0.14	22.16 ± 0.09	20.52 ± 0.05	18.44 ± 0.13	17.28 ± 0.20
2	$16^h08^m59.8^s$	54°57′11.2″	>25.00	22.53 ± 0.05	21.18 ± 0.03	20.01 ± 0.04	18.59 ± 0.19	16.64 ± 0.14
3	$16^h09^m10.5^s$	54°56′37.8″	>25.00	23.65 ± 0.14	22.56 ± 0.10	21.08 ± 0.10	19.46 ± 0.27	17.60 ± 0.26
4	$16^h10^m26.7^s$	55°04′07.5″	24.80 ± 0.16	23.23 ± 0.11	21.90 ± 0.05	20.52 ± 0.06	18.96 ± 0.20	17.15 ± 0.24
5	$16^h10^m33.8^s$	55°09′33.2″	>25.00	>24.10	22.36 ± 0.08	20.92 ± 0.00	18.92 ± 0.27	17.40 ± 0.22
6	$16^h10^m41.2^s$	54°13′31.0″	>25.00	23.07 ± 0.09	21.96 ± 0.07	20.90 ± 0.07	19.50 ± 0.35	17.32 ± 0.22
7	$16^h10^m42.8^s$	55°01′26.8″	>25.00	23.33 ± 0.12	21.94 ± 0.05	20.49 ± 0.06	19.07 ± 0.25	17.21 ± 0.21
8	$16^h10^m45.2^s$	55°04′50.1″	23.84 ± 0.07	22.34 ± 0.05	21.42 ± 0.03	20.60 ± 0.06	18.89 ± 0.24	16.71 ± 0.15
9	$16^h11^m19.1^s$	55°07′46.5″	>25.00	23.57 ± 0.14	22.28 ± 0.07	21.22 ± 0.10	19.56 ± 0.33	17.25 ± 0.23
10	$16^h12^m15.3^s$	54°53′38.0″	>25.00	23.96 ± 0.00	22.42 ± 0.00	20.93 ± 0.09	18.92 ± 0.27	17.34 ± 0.24
11	$16^h35^m12.2^s$	40°48′35.9″	24.58 ± 0.15	22.63 ± 0.06	21.14 ± 0.04	19.68 ± 0.04	18.67 ± 0.27	16.71 ± 0.16
12	$16^h34^m45.9^s$	40°48′26.2″	>25.00	23.58 ± 0.14	22.10 ± 0.10	20.90 ± 0.08	19.44 ± 0.27	17.69 ± 0.25
13	$16^h36^m17.9^s$	41°15′39.8″	>25.00	23.40 ± 0.13	21.87 ± 0.09	20.78 ± 0.10	19.09 ± 0.24	17.12 ± 0.16
14	$16^h36^m52.8^s$	40°53′55.8″	>25.00	>24.10	22.39 ± 0.00	20.82 ± 0.07	18.63 ± 0.18	16.71 ± 0.14
15	$16^h37^m39.6^s$	40°53′17.0″	>25.00	23.65 ± 0.13	21.92 ± 0.08	21.49 ± 0.11	19.47 ± 0.31	17.43 ± 0.25
16	$16^h38^m01.3^s$	40°56′59.6″	>25.00	>24.10	22.36 ± 0.00	19.52 ± 0.02	18.69 ± 0.22	16.95 ± 0.16
17	$16^h38^m33.7^s$	41°07′52.0″	>25.00	>24.10	22.44 ± 0.13	21.07 ± 0.00	19.61 ± 0.30	17.41 ± 0.24
18	$16^h06^m52.7^s$	54°46′37.3″	>25.00	22.49 ± 0.05	21.06 ± 0.03	20.29 ± 0.03	18.75 ± 0.19	16.89 ± 0.20
19	$16^h08^m15.6^s$	54°41′51.7″	>25.00	22.60 ± 0.06	20.94 ± 0.03	20.02 ± 0.03	19.03 ± 0.23	17.07 ± 0.17
20	$16^h08^m38.7^s$	55°00′19.5″	>25.00	23.14 ± 0.09	21.52 ± 0.04	20.45 ± 0.06	18.88 ± 0.24	17.29 ± 0.26
21	$16^h08^m59.4^s$	54°56′34.1″	24.72 ± 0.17	22.84 ± 0.07	21.33 ± 0.03	20.08 ± 0.04	19.06 ± 0.20	17.10 ± 0.18
22	$16^h08^m60.0^s$	54°56′25.7″	>25.00	22.84 ± 0.07	21.41 ± 0.04	20.17 ± 0.05	19.16 ± 0.23	17.12 ± 0.19
23	$16^h10^m21.0^s$	55°07′28.1″	24.72 ± 0.15	22.86 ± 0.08	21.14 ± 0.03	20.32 ± 0.05	18.83 ± 0.17	17.24 ± 0.24
24	$16^h10^m30.3^s$	55°08′21.1″	24.58 ± 0.13	22.73 ± 0.07	21.47 ± 0.03	20.99 ± 0.09	18.83 ± 0.19	17.18 ± 0.20
25	$16^h10^m40.4^s$	55°05′25.7″	24.31 ± 0.11	22.72 ± 0.07	21.16 ± 0.03	20.20 ± 0.04	18.88 ± 0.23	17.18 ± 0.21
26	$16^h10^m51.0^s$	55°12′05.8″	24.29 ± 0.11	22.99 ± 0.08	21.75 ± 0.04	21.04 ± 0.09	19.31 ± 0.33	17.47 ± 0.24
27	$16^h10^m59.1^s$	54°31′26.2″	>25.00	22.90 ± 0.07	21.28 ± 0.04	20.15 ± 0.03	19.00 ± 0.55	17.25 ± 0.23
28	$16^h11^m08.9^s$	54°50′17.7″	>25.00	23.07 ± 0.07	21.64 ± 0.05	20.85 ± 0.06	19.42 ± 0.31	17.42 ± 0.24
29	$16^h11^m12.8^s$	55°08′24.7″	23.43 ± 0.05	22.57 ± 0.06	21.25 ± 0.03	20.17 ± 0.04	18.73 ± 0.24	16.91 ± 0.17
30	$16^h11^m14.7^s$	55°05′31.8″	>25.00	23.02 ± 0.09	21.43 ± 0.03	20.75 ± 0.07	19.09 ± 0.26	17.07 ± 0.21
31	$16^h11^m58.4^s$	54°53′56.5″	>25.00	22.91 ± 0.08	21.50 ± 0.04	20.50 ± 0.05	18.93 ± 0.24	17.40 ± 0.23
32	$16^h34^m14.4^s$	41°14′42.5″	24.49 ± 0.16	22.32 ± 0.04	20.71 ± 0.03	19.91 ± 0.03	18.81 ± 0.27	16.59 ± 0.26
33	$16^h34^m22.8^s$	40°56′07.1″	>25.00	22.76 ± 0.06	20.96 ± 0.04	20.23 ± 0.04	19.13 ± 0.26	17.12 ± 0.23
34	$16^h34^m52.1^s$	40°50′50.2″	>25.00	23.02 ± 0.08	21.41 ± 0.05	20.57 ± 0.05	19.05 ± 0.23	17.39 ± 0.20
35	$16^h34^m58.4^s$	40°52′55.4″	>25.00	22.80 ± 0.06	21.10 ± 0.04	20.36 ± 0.04	18.86 ± 0.19	17.20 ± 0.16
36	$16^h35^m12.1^s$	40°47′31.0″	>25.00	23.31 ± 0.11	21.82 ± 0.08	20.69 ± 0.07	19.13 ± 0.27	17.60 ± 0.25
37	$16^h36^m01.0^s$	41°05′59.3″	>25.00	22.99 ± 0.08	21.58 ± 0.06	20.30 ± 0.05	19.01 ± 0.17	17.22 ± 0.21
38	$16^h36^m07.5^s$	41°21′42.3″	24.69 ± 0.00	22.39 ± 0.04	20.97 ± 0.00	19.95 ± 0.00	19.11 ± 0.27	16.74 ± 0.23
39	$16^h36^m07.8^s$	41°03′41.4″	>25.00	22.94 ± 0.07	21.35 ± 0.07	20.78 ± 0.07	19.56 ± 0.27	17.24 ± 0.23
40	$16^h36^m58.1^s$	40°49′43.9″	>25.00	22.41 ± 0.05	20.74 ± 0.03	19.95 ± 0.03	18.64 ± 0.20	16.72 ± 0.11
41	$16^h37^m23.9^s$	41°01′16.0″	>25.00	23.27 ± 0.10	21.42 ± 0.09	20.66 ± 0.05	19.19 ± 0.27	17.64 ± 0.26
42	$16^h37^m27.5^s$	40°55′43.6″	>25.00	23.03 ± 0.00	21.27 ± 0.00	20.90 ± 0.08	18.97 ± 0.24	17.45 ± 0.26
43	$16^h37^m31.0^s$	40°53′36.3″	23.93 ± 0.10	22.47 ± 0.05	20.76 ± 0.03	19.99 ± 0.03	18.57 ± 0.20	16.79 ± 0.16
44	$16^h37^m38.6^s$	40°56′59.3″	>25.00	23.00 ± 0.07	21.36 ± 0.05	20.39 ± 0.04	19.19 ± 0.40	17.10 ± 0.17
45	$16^h37^m40.2^s$	40°54′21.8″	>25.00	22.64 ± 0.05	20.80 ± 0.05	19.66 ± 0.05	18.86 ± 0.23	17.10 ± 0.20
46	$16^h37^m49.6^s$	40°55′43.5″	>25.00	22.66 ± 0.05	20.86 ± 0.03	20.12 ± 0.03	18.92 ± 0.24	16.98 ± 0.17
47	$16^h37^m57.2^s$	41°19′38.4″	24.18 ± 0.00	23.09 ± 0.08	21.57 ± 0.06	20.75 ± 0.08	19.65 ± 0.31	17.45 ± 0.22
48	$16^h37^m58.1^s$	41°09′47.6″	24.24 ± 0.12	22.80 ± 0.06	21.48 ± 0.05	20.56 ± 0.06	19.40 ± 0.28	17.15 ± 0.19
49	$16^h38^m20.3^s$	41°03′42.5″	23.73 ± 0.08	22.21 ± 0.04	20.55 ± 0.02	19.76 ± 0.03	18.72 ± 0.31	16.62 ± 0.23
50	$16^h38^m46.1^s$	41°08′18.8″	>25.00	23.37 ± 0.10	21.64 ± 0.06	20.48 ± 0.06	19.39 ± 0.29	17.27 ± 0.24
51	$16^h10^m35.1^s$	55°10′04.0″	23.55 ± 0.06	22.69 ± 0.06	21.89 ± 0.05	20.92 ± 0.08	19.36 ± 0.35	17.47 ± 0.26
52	$16^h11^m13.3^s$	54°52′48.3″	22.86 ± 0.05	21.99 ± 0.06	21.34 ± 0.04	20.18 ± 0.04	18.65 ± 0.17	16.94 ± 0.17
53	$16^h34^m21.4^s$	40°57′56.2″	23.96 ± 0.09	22.96 ± 0.08	22.19 ± 0.10	21.21 ± 0.10	19.35 ± 0.28	17.50 ± 0.25
54	$16^h35^m46.0^s$	41°14′38.6″	23.66 ± 0.15	22.64 ± 0.08	22.02 ± 0.08	20.98 ± 0.07	19.76 ± 0.28	17.18 ± 0.22

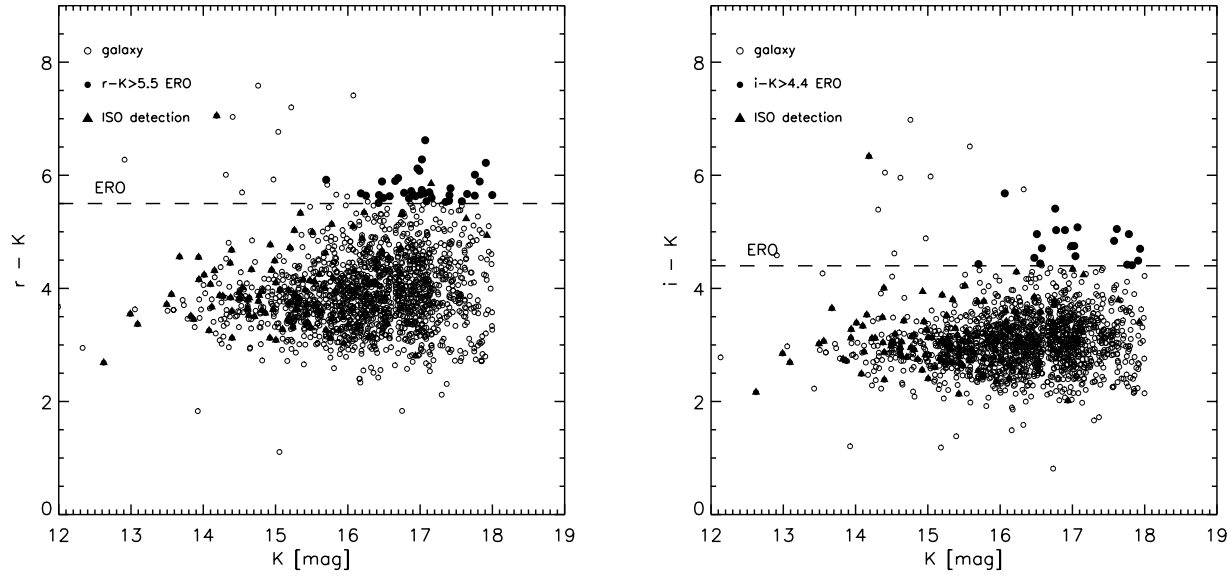

Fig. 3. The K-band magnitude vs. the $r-K$ and $i-K$ colours, in left and right panels, respectively. All objects coming through the catalogue construction as galaxies are plotted as open circles. Individually verified EROs at $>5\sigma$ level are overlaid with solid circles. Since the survey was done in ELAIS fields, we also overplot all matched ISOCAM detections as solid triangles. Note that the total K-magnitude is used on the x-axis, whereas the colour is calculated with matching small apertures.

Table 2. Columns (2) to (5) give the total numbers of sources and stellar objects, the surveyed area, and the average limiting magnitude. The rest of the columns refer to galaxies only: Cols. (6) to (7) give mean colours, though note that these are lower limits since optical non-detections we ignored. Column (8) gives the number of EROs selected by $r-K \geq 5.5$; (9) by $i-K \geq 4.4$; and (10) by their combination; Col. (11) is the range of surface densities resulting from either r or i band based selection; Col. (12) is the range of cumulative surface densities at $K < 17$.

Sample	N	$N_\star$	Area arcmin^2	$K_{\rm lim}$	$\langle r-K \rangle$	$\langle i-K \rangle$	EROs			ERO/arcmin^2	
(1)	(2)	(3)	(4)	(5)	(6)	(7)	(8)	(9)	(10)	(11)	(12)
Mt.Hopkins	6618	3306	2850	17.5	3.91	3.09	50	21	17	0.007–0.018	0.004–0.007

We wish to point out, that in order to be very conservative in limiting the number of spurious detections in final ERO lists, as well as to be able to take advantage of the $J-K$ colour in classifiying EROs, we required both a J and a K detection for all considered objects from the survey. While the 5σ detection requirement was applied only to the K-band, this nevertheless might exclude some genuine EROs which are very red in $J-K$ colour. At our faintest levels of $K \geq 17.5$, we do not expect to detect any $J-K \geq 2.5$ EROs, and already at $K \geq 17$ the completeness of $J-K \geq 2$ EROs would not be quite as high as $J-K < 2$ EROs.

4. Separation of dusty EROs

Since the Extremely Red Objects can be divided into two broad classes, the populations should be differentiated before surface density comparisons to detailed galaxy formation models are attempted. A prime motivation of this study is to attempt the separation using the mid-IR data. We shall also perform the separation using other established methods, and discuss the differences.

4.1. Using mid-IR data

Since only dusty EROs are expected to show up in the mid-IR ELAIS survey, the question to answer is, what fraction of the EROs are detected in the mid-IR *to a given flux limit*?

Among the 54 Mt.Hopkins EROs we find only one match with a 15 μm ISOCAM source. In the ELAIS band-merged catalogue (Rowan-Robinson et al. 2004) the source is a candidate hyper luminous IR-galaxy based on a photometric redshift of $z \approx 1.0$, which agrees with our independent photometric redshift determination of $z = 0.9$. (We note that using the same near-IR data-set but with only K-band considered, another ISOCAM detected ERO is found in Rowan-Robinson et al. 2004.) Thus, at face value, the fraction of dusty EROs seems to be insignicant.

However, it is crucial to take into account detection limits. The main hindrance to the full power of the mid-IR separation with our data-set is the relative shallowness of the ELAIS survey. All the Mt.Hopkins EROs have $K = 16-18$ mag. Comparing to GRASIL models (Fig. 1), a starburst galaxy with M 82-type SED and $K = 17$ apparent magnitude should just have been detected over the 0.7 mJy ISOCAM flux limit.

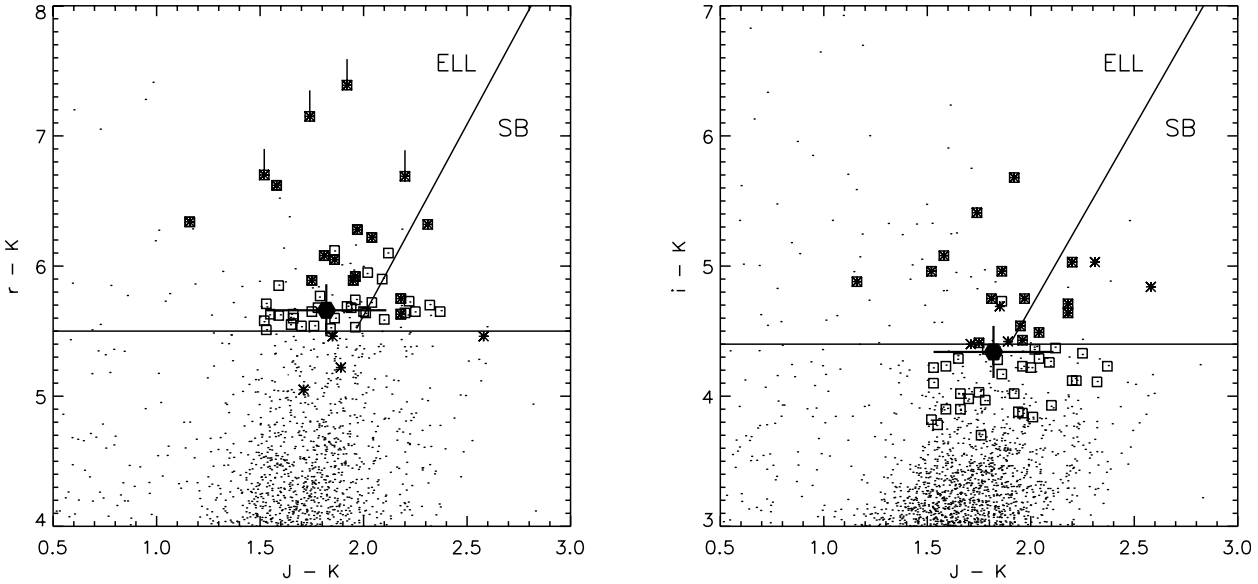

Fig. 4. $J-K$ vs. $r-K$ and $i-K$ ERO discriminator colours adopted from Pozzetti & Mannucci (2000). All galaxies are plotted as dots and EROs are overlaid with larger symbols. Squares are $r-K > 5.5$ EROs and asterisks $i-K > 4.4$ EROs. Those $i-K$ EROs with no r-band detection have lower limits indicated in the left panel. The only mid-IR detected ERO is shown as the large solid symbol – its error bars are representative to errors of all EROs.

In comparison, to detect the Rayleigh-Jeans tail of ellipticals would have required approximately $K = 13$ brightness. We note that M 82-type galaxy with $K = 17$ mag at $z = 0.7$ and $z = 1.0$ translates to star formation rates $SFR \approx 100$ and 200 $M_\odot$ yr^{-1}, respectively, as calculated from total IR luminosity $L_{\rm IR}(3-1000\ \mu{\rm m})$ with relation given in Mann et al. (2002) and using the GRASIL model SED. The corresponding IR luminosities are $\log(L_{\rm IR}) > 11.7$.

There are 23 K < 17 EROs in the sample, out of which only one (4%) is detected in the mid-IR. As shown above, the ELAIS data is only sensitive to luminous IR galaxies at the expected redshifts of EROs ($z > 0.7$). Thus, we can state that very strong starbursts ($SFR > 100\ M_\odot$ yr^{-1}) make up only a small fraction, less than 10%, of counterparts to bright EROs. For detection of more modest dusty galaxies other methods have to be used.

It is relevant to note that the in-orbit Spitzer mission will definitely find large numbers of dusty EROs, including more modest ones than above: using the M 82 SED once again as an example, sampling dusty $K \approx 20$ EROs at $z \approx 1$ would mean probing dusty starforming galaxies of $SFR \sim 10\ M_\odot$ yr^{-1}. The expected flux densities of such objects with IRAC 8 μm and MIPS 24 μm bands would be of the order of 10 and 150 μJy, respectively, which are easily reached in a few minutes of integration time. For example, assuming 10 min per pixel integrations, a 10 h survey to the mentioned 5σ depths would cover ~800 arcmin^2 in both bands. This means detecting 100–200 MIR counterparts of dusty EROs, assuming average ERO surface densities and an ad hoc 50% fraction of dusty EROs.

4.2. Colour–colour selections

Figure 4 shows the colour–colour separation scheme of EROs by Pozzetti & Mannucci (2000) adopted for our r, i filters. The idea is that the $J-K$ separates the EROs at $z > 1$ to bluer early type galaxies (where the large optical to near-IR colour is due to the 4000 Å break), and to the redder (in $J-K$) dusty EROs which have a a smoother SED from optical to near-IR. In the $r-K$ plot we find 9/50 $r-K$ selected EROs in the dusty starburst side of the indicator, and similarly 3/16 of the $i-K$ EROs. In the $i-K$ plot many $r-K$ EROs fall under the $i-K = 4.4$ line, and the dusty percentages are higher for the remaining EROs, 30–50%. The one mid-IR ERO is overplotted in the figure, and it in fact falls on the elliptical side of the division. However, given the typical photometric errors of the EROs (the error bars on the mid-IR ERO are representative) it is seen that at least 1/3 of the EROs fall statistically on the dividing line. Moreover, while the elliptical vs. starburst separating line is equivalent to Pozzetti & Mannucci, it is only defined to work for $R-K > 5.3$. If we thus select EROs at $r-K > 5.8$, nearly all galaxies on the starburst side of the left panel in Fig. 4 fall out, and the elliptical fraction becomes close to 90%. Finally, our Mt.Hopkins sample is 1–2 mag brighter than other typical ERO samples, and it is therefore not certain how accurate the separation should be.

We also checked the colour–colour separation scheme presented by Bergström & Wiklind (2004) using $R-J$ vs. $J-K$ colours (see their Fig. 8). The result is 85% ellipticals regardless of whether $r-K$ or $i-K$ ERO criterion (or both) is used, totally consistent with the fractions emerging from the Pozzetti & Mannucci $R-K$ vs. $J-K$ method.

We thus conclude that using the various $J-K$ vs. optical-NIR colour separation schemes approximately 80% of our EROs appear ellipticals. Only when using Pozzetti & Mannucci $i-K$ based separation for $i-K > 4.4$ EROs, is the percentage lower, ≈60%. We might be missing the very reddest $J-K$ EROs, i.e. some dusty EROs, because of the selection of the sample in both bands. At $K < 17$, where there should be

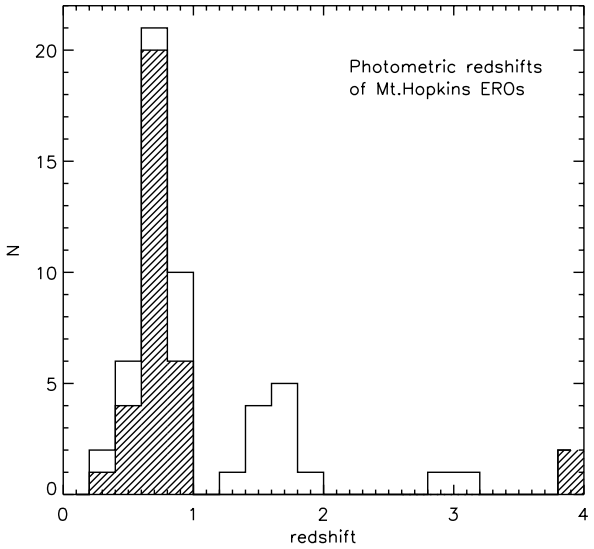

Fig. 5. Photometric redshifts as calculated by HYPERZ. All 54 Mt.Hopkins EROs are plotted, whatever the confidence of the fit (half have >85%). $r-K>5.5$ selected EROs which are *not* EROs with $i-K>4.4$ selection are hatched, the empty regions of the histogram thus show the $i-K>4.4$ EROs.

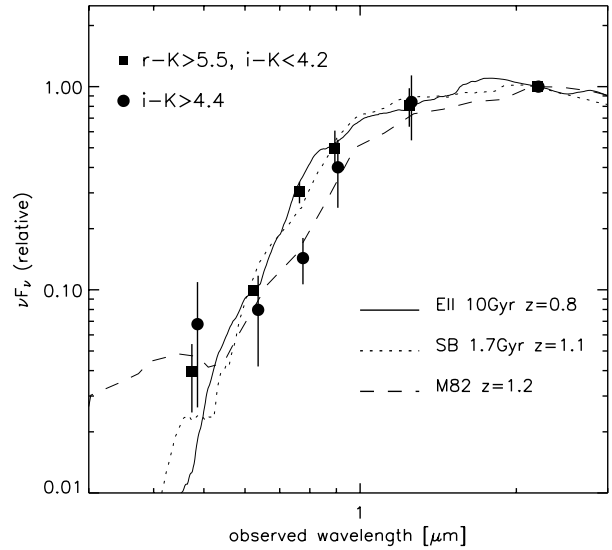

Fig. 6. Averaged and K-band normalized SEDs of $i-K$ EROs (circles) and those $r-K$ EROs with $i-K<4.2$ (squares). The observed bands are g, r, i, Z, J, K. The GRASIL M 82 model and elliptical and evolved starburst SEDs from BC are also plotted at indicated redshifts.

no bias in $J-K$ colour, the fractions of early type EROs range between 65−80%, depending on the optical band used.

5. Photometric redshifts and SEDs

We calculated photometric redshifts for the EROs using the HYPERZ code (2000) which fits GISSEL98 synthetic spectra (Bruzual & Charlot 1993; BC hereafter) galaxy templates to photometric data points. Figure 5 shows the photometric redshift distributions of our sample. The mean photometric redshift is $z = 0.94 \pm 0.49$, excluding the outliers at $z \sim 4$. However, it is clear that subgroups are involved, though the gap at $z = 1$−1.2 is difficult to understand. We also note that approximately half of the fits result in a confidence better than >85%, so the results should be taken with some caution. On the other hand, the overall distribution, average redshifts, or properties of sub-groups discussed below do not change if we consider only those EROs with fits of >85% confidence.

The 21 $i-K$ selected EROs, the white regions in the histogram, are more evenly distributed and at higher z (average $z \approx 1.4$) than $r-K$ EROs. The 17 objects which are EROs with both selection criteria cover quite evenly the range $z = 0.6$−1.8 (average at $z \approx 1.3$). The EROs #51–54 in Table 1 are all between $z = 1.4$−1.9.

Most notably, however, those EROs that are *not* EROs with the $i-K>4.4$ criteria, show a significantly narrower redshift distribution (hatched region of histrogram) with $z = 0.73 \pm 0.06$. Moreover, these objects constitute more than half, 33/54, of our total ERO sample – we return to these below in Sect. 6.2. Taken together, the photometric redshifts thus suggest that $r-K>5.5$ selects more nearby systems at redshift unity and below, and $i-K>4.4$ includes a wider range of EROs.

Virtually all, 50/54, of the best-fit HYPERZ BC SEDs are either starburst spectra of age 0.4 to 2 Gyr, or elliptical spectra at several Gyr – these SEDs are nearly identical (see Fig. 6). In fact, in a recent paper by Pierini et al. (2004) it was proposed that post-starburst ellipticals, forming in a short bursts *during* the period where EROs are observed (between $1 < z < 2$), are a neglected constituent of ERO populations. It should be stressed that basically all of the best-fit HYPERZ "starbursts" are evolved results of instantenious bursts and not dusty star-forming galaxies.

6. Discussion

6.1. ERO counts and surface densities

The numbers of detected EROs are given in Table 3, and the corresponding cumulative number counts are plotted in Fig. 7. The numbers plotted are the total ERO counts: based on the previous discussion, the fraction of dusty EROs is low (∼15%) and does not have significant effect even if subtracted from the counts.

Our wide survey from Mt.Hopkins extends the ERO number counts to brighter magnitudes than observed before. We report the first ERO counts at $K<16.5$, where the $r-K>5.5$ (i.e. $R-K>5$) selection yields a surface density of 0.002 ± 0.001 arcmin^2, and the $i-K>4.4$ (i.e. $I-K>4$) selection ≈50% of this value. At $K<17$ mag we arrive at 0.007 ± 0.002 arcmin^2 of $r-K$ EROs. Beyond $K>17$ mag the Mt.Hopkins survey is starting to be affected by incompleteness, and based on simulations performed in V00 for the same dataset, we estimate a factor of 1.5 correction to the $K<17.5$ cumulative ERO density. The resulting $r-K$ selected surface density at $K<17.5$ is 0.018 ± 0.003 arcmin^2.

We compare these numbers to the only two other field ERO surveys with enough sky coverage to reach these bright magnitude levels: the largest ERO survey to date Daddi et al. (2000a; with 701 arcmin^2), yielded 0.003 ± 0.002 arcmin^2 at

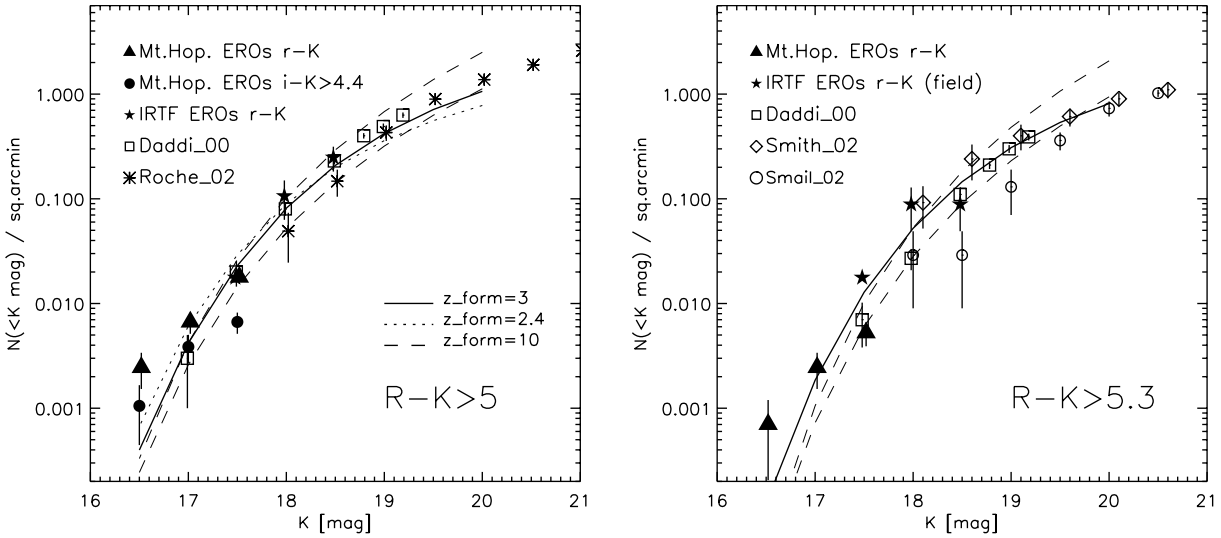

Fig. 7. Cumulative ERO counts are shown for $R-K>5$ and $R-K>5.3$ selections (i.e. $r-K>5.5$ and $r-K>5.8$), in the left and right panels, respectively, with solid triangles. Additionally, the $i-K>4.4$ selected EROs are plotted in the left panel with circles. Error bars are Poissonian. Our other field ERO counts from a deeper survey (IRTF, Väisänen & Johansson 2004) are shown as stars. Squares show the EROs of Daddi et al. (2000a) and the asterisks the Roche et al. (2002) EROs in the left panel. The left panel shows $R-K>5$ selected EROs of Daddi et al. (2000a) and Roche et al. (2002). In addition to the Daddi et al. (2000a) $R-K>5.3$ selected EROs the right panel plots the corresponding Smith et al. (2002) and Smail et al. (2002) EROs. We plot PLE models of Daddi et al. (2000b) calculated using the indicated $R-K$ cuts. The curves are different by their galaxy formation redshifts, as indicated in the figure. The two dashed-lines employ a different LF – the higher curve results from a 2MASS normalized LF, and the lower from that of Marzke et al. (1994).

Table 3. The sample of Mt.Hopkins EROs. Cumulative counts are given for different ERO colour selection criteria. Total numbers (N), Fraction of EROs compared to the total galaxy count ("Frac.") is calculated using galaxy counts in these same fields (Väisänen et al. 2000). At $K \leq 17.5$ N shows the completeness corrected value, and the raw count is given in parentheses.

	$r-K>5.5$			$r-K>5.8$			$i-K>4.4$		
K limit (mag)	N	Frac. %	Σ_K arcmin^{-2}	N	Frac. %	Σ_K arcmin^{-2}	N	Frac. %	Σ_K arcmin^{-2}
$K \leq 16.5$	7	0.004	0.002	2	0.001	0.0007	3	0.002	0.001
$K \leq 17.0$	19	0.008	0.007	7	0.003	0.002	11	0.005	0.004
$K \leq 17.5$	51 (35)	0.012	0.018	15 (11)	0.004	0.005	19 (15)	0.005	0.007

$K < 17$ and 0.02 ± 0.006 arcmin^2 at $K < 17.5$. These are totally consistent with our result.

The Yan & Thompson (2003; 409 arcmin^2) HST ERO counts were selected using $I-K>4.0$. At $K<17$ they agree with our corresponding $i-K>4.4$ selection within the errors. At $K<17.5$ there is a clear discrepancy, however. It is our $r-K$ selected EROs which are in closer agreement with the Yan & Thompson ERO counts – we systematically find a factor of ∼2 less $i-K$ selected EROs than $r-K$ selected ones. Especially at the faintest bin there appears to either be more incompleteness than we expect, or the $i-K>4.4$ selection does not pick up as many bright $K \sim 17$ galaxies at $z \sim 1$ than the $r-K$ selection does. Indeed, the discussion on "excess" $r-K$ EROs in the next Sect. 6.2 and the photometric redshifts derived for the EROs hint at the latter possibility.

6.2. Evolved ellipticals at $z \sim 1$

The strength, and motivation, of ERO searches has been to look for the most massive galaxies at redshifts of unity and over (see e.g. Saracco et al. 2003), since it is exactly these which place tight constraints on galaxy formation scenarios. The dusty vs. early type ERO discriminators showed that most of our ERO sample is consistent with being early type galaxies. However, we argue that the clearest population of ellipticals comes from the class of $r-K>5.5$ EROs which have $r-K<4.4$ – these constitute 60% of all our EROs. Figure 8 shows an $i-K$ vs. $r-K$ plot, where these "excess" EROs populate the upper right quadrant (see also Figs. 4 and 6).

Intuitively, the upper left quadrant galaxies should be sources at a redshift where a significant 4000 Å break falls right in between the r and i bands: i.e. ellipticals or very early type spirals at a redshift $z \sim 0.8$. We calculated numerous GRASIL models, and it turns out to be fairly difficult to obtain colours in this ERO regime. Any significant on-going star-formation drops the $r-K$ colour down, as noted also by e.g. Yan & Thompson (2003; see their Fig. 9). The effect is seen in the solid curve of the right panel of Fig. 8: the elliptical model has a formation redshift of $z_\star = 3$ and at redshifts of $z > 1.5$ the effects of the starburst turn the $r-K$ colour sharply down.

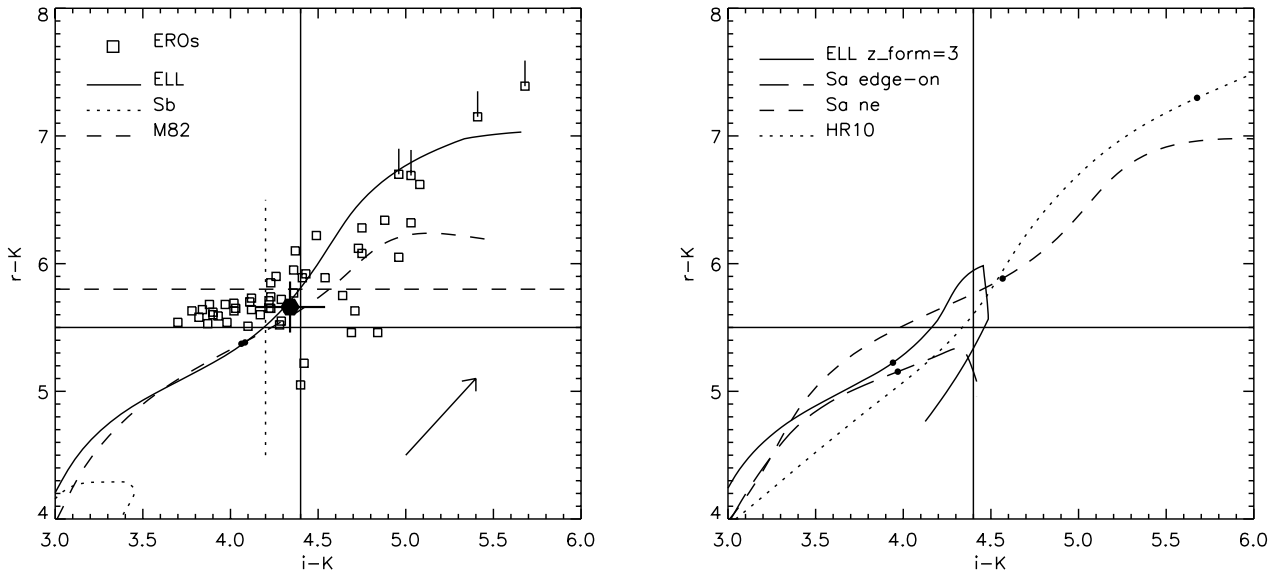

Fig. 8. $i - K$ vs. $r - K$ colour−colour magnitude diagramme of the verified EROs is plotted in the left panel. The mid-IR detected EROs is overplotted as a large solid symbol. Several GRASIL models are plotted in both panels: the models are drawn until redshift $z = 2$, and the $z = 1$ locations are indicated by small solid circles along the curves. The reddening direction is indicated in the left panel by the diagonal arrow which correcponds to $A_V = 1$ extinction.

Significant amounts of extinction, including edge-on spirals, do not bring models to the $r - K > 5.5, i - K < 4.4$ region either: the dotted line depicts the extremely dusty HR10 model as an example.

One gets closest to the $r - K > 5.5$, $i - K \sim 4$ region by merely redshifting an old present-day elliptical to Sa galaxy to the appropriate redshift. This is shown as the dashed curve, a 13 Gyr old Sa spiral; any >10 Gyr old elliptical produces a similar result. While this is an unphysical model, it serves to point out that while pure reddening is unlikely to reach this part of the colour−colour diagramme, an old stellar population does that. We thus conclude that EROs which are selected by $r - K > 5.5$ (i.e. $R - K > 5$) which are not EROs by $i - K > 4.4$ (i.e. $I - K > 4$) are mostly early type galaxies. In fact, at $i - K < 4.2$ there should not be any contamination from dusty galaxies (compare the vertical dotted line to the dusty model curves).

We also plot a sample of averaged SEDs of our EROs in Fig. 6. The "excess" EROs with $i - K < 4.2$ are plotted with squares and are well fit by very evolved galaxy SEDs, as just discussed. The critical observed band is the i band, where the difference between elliptical and dusty starbursts (M 82 plotted) is the largest at the redshifts of our targets. Note that the g-band is biased to the bluest sources, since the average is calculated from those EROs detected in the corresponding band, and only 25% of the sources have a g-band detection.

The $r - K$ and $i - K$ selections alone are quite different (see e.g. Scodeggio & Silva 2000). At least with bright ERO surveys such as ours, it seems that $r - K$ selects more passive systems. This is consistent with spectroscopic followup of $R - K > 5.3$ surveys finding significant amounts of ellipticals (e.g. Cimatti et al. 2002) and those following up $I - K > 4$ selections finding much more star formation (e.g. Yan et al. 2004).

6.2.1. Number densities

There are 33 "excess" $r - K$ EROs with $i - K < 4.4$. They appear to be at redshifts $z = 0.7$−1.2: BC SED fitting favours redshifts below unity (Fig. 5), while the GRASIL models suggest redshifts at $z \approx 1$−1.2 (e.g. Fig. 8). These EROs have typical magnitudes of $K \approx 17.2$, which would make them at least $\sim 2\ L^\star$ galaxies, taking into account passive evolution since that redshift. Very simply, assuming that this group of EROs consists of ellipticals and is constrained in the mentioned redshift range we derive a co-moving volume of 2×10^6 Mpc^3 for the Mt.Hopkins survey area, and thus a space density of $\sim 2 \times 10^{-5}$ Mpc^{-3}. Taking K-band LF parameters from Kochanek et al. (2001), this is a significant part of the expected density of $\approx 8 \times 10^{-5}$ Mpc^{-3} for local >2 $L^\star$ early type galaxies. Given the incompleteness in our survey at $K > 17$, and that we did not include ellipticals at $i - K > 4.4$ in this calculation these ERO counts are a very conservative lower limit, and thus indicate that a major part of massive present day ~ 2−3 $L^\star$ ellipticals were in place at $z \sim 1$ (e.g. Totani et al. 2001; Saracco et al. 2003).

The space density just derived is intriguingly close to those estimated for the higher redshift sub-mm population, which are suspected to be the most luminous starbursts, perhaps the progenitors of present day massive ellipticals (see e.g. discussion in Scott et al. 2002).

6.3. Constraints on galaxy formation scenarios

Figure 7 plots our ERO counts along with several other recent surveys and pure luminosity evolution (PLE) models of Daddi et al. (2000b). All curves depict ellipticals with a $\tau = 0.1$ Gyr initial starburst, and passive evolution afterwards.

The different lines have formation redshifts of $z_{\rm form} = 2.4, 3.0$, and 10. All the models use a Marzke et al. (1994) LF, except the uppermost dashed line, which instead uses a 2MASS based LF (Kochanek et al. 2001) resulting in a higher normalization by approximately a factor of two.

We stress that *all EROs are counted* in the figure, i.e. no corrections for the dusty population have been made. As was seen previously, this is perfectly reasonable for our very bright sample of EROs. However, even a very large correction (not supported by our observations) of 50% of the EROs being in fact dusty, would not change the conclusion significantly. At somewhat fainter magnitudes, recent studies have shown (Cimatti et al. 2002; Smail et al. 2002) that the percentage of dusty EROs is likely somewhere around 30−60%.

The PLE model using a formation redshift of $z_{\rm form} = 3$ fits all the data remarkably well. Formation redshifts slightly lower than this also fit well our bright ERO counts, but start underpredicting the numbers at fainter magnitudes. On the other hand, corrections for dusty galaxies might be larger at the fainter levels (see e.g. Smith et al. 2002). However, models with $z_{\rm form} < 2.4$ start underpredicting the counts at all levels, especially when using the $R - K > 5.3$ selection criteria. The very highest formation redshifts of $z_{\rm form} = 10$ and over, predict steeper number counts and are more difficult to fit to both the bright and faint end of ERO counts with the same normalization. The figure shows two different LFs giving a factor of ∼2 difference. Note also that eventhough the $R - K > 5.3$ criterion eliminates nearly all the (possibly) lower redshift $z \sim 0.8$ EROs, there is no significant difference in the fits of PLE models in the right and left panels of Fig. 7.

Using the 2MASS normalized LF it is in fact slightly more difficult to fit both $R - K > 5$ and $R - K > 5.3$ counts simultaneously. The $R - K > 5$ counts are overpredicted by a factor of 1.5−3 with all except the very lowest $z_{\rm form} = 2.2$−2.4 formation redshifts. Good fits in the range $K = 16.5$−18.5 are again acquired with $z_{\rm form} \geq 4$, but the faintest counts are overpredicted. Roche et al. (2002, 2003) find their 2MASS-LF based PLE models significantly overpredicting $I - K > 4$ ERO counts, and show that certain amount of merging and density evolution fits the counts much better in particular in the fainter $K > 20$ regime.

That a range of formation redshifts are necessary to model EROs is seen for example by comparing Figs. 8 and 7 (see also Cimatti et al. 2003): though models with formation redshifts of $z \approx 3$ fit well the *counts*, the *colours* produced by such a scenario are not red enough for many EROs found in this survey, and others. Very red colours of $r - K > 6.5$ or $i - K > 5$ can not be produced without pushing $z_{\rm form}$ closer to 10 (unless all such extreme EROs are heavily reddened starbursts).

We do not investigate hierarchical formation scenarios in more detail here. We merely point out that predictions from some recent models (Cole et al. 2000 as presented in Smith et al. 2002), fall short an order of magnitude in the numbers of EROs in the range $K = 17$−20. See also e.g. discussion by Martini (2001) and Firth et al. (2002). It is important to realize that a drastic increase in the fraction of dusty EROs does not make the hierarchical models fit the ERO counts any better: they predict too few EROs of all kinds. On the other hand large fractions of dusty EROs would have to be subtracted from PLE models including only ellipticals, making all the Daddi et al. (2000b) PLE models used above to overpredict the counts by factors of 1.5−3.

It is concluded that the PLE models do give remarkably good fits to the brightest ERO counts. Formation redshifts around $z \sim 3$ are favoured – however, by altering the details of the models, formation redshifts between $z = 2$−10 are also consistent. Moreover, a range in the formation era of ellipticals is suggested by the range in ERO colours.

7. Summary

We have searched for EROs in a near-IR survey performed in ELAIS fields, using $r - K > 5.5$, $r - K > 5.8$, and $i - K > 4.4$ colour criteria. These are equivalent to the commonly used $R - K > 5$, $R - K > 5.3$, and $I - K > 4$. In the survey, reaching approximately $K = 17.5$, we find 54 EROs. The area covered is 2850 arcmin^2.

Taking advantage of overlapping mid-IR data, we search for dusty EROs, since only these should be detected with the used 15 μm ISOCAM band. Only one is found from our conservatively constructed catalogue. Taking into account detection limits we limit the number of very strong starbursts ($SFR \geq 200\ M_\odot\ {\rm yr}^{-1}$) in the bright $K < 17$−17.5 ERO population to <10%.

We also make use of a $J - K$ vs. optical-infrared colour−colour diagramme to separate EROs, and find that the fraction of dusty ERO population is <10−40%, depending on the colour used. There are more dusty galaxies in the $i-K$ based ERO selection than if $r-K$ is used. HYPERZ photometric redshifts and template fits are also employed: nearly all redshifts are in the range $z = 0.6$−1.8 with a strong peak at $z \sim 0.8$. Approximately 90% of the best-fit SEDs are those of evolved stellar populations.

We find a considerable amount, ∼60% of all our EROs, of $r-K > 5.5$ EROs which are not EROs with the $i-K > 4.4$ criterion. Using models we interpret these to be early type galaxies at redshift of $z \sim 0.7$−1.1. They are interpreted to be the counterparts of local 2−3 $L^\star$ galaxies, and their resulting space density is approximately $2 \times 10^{-5}\,{\rm Mpc}^{-3}$.

Cumulative number counts are provided for the EROs, extending the available ERO counts to brighter limits than previously. Our counts are consistent with literature counts in the overlapping magnitude region with same colour cut-offs.

Our ERO number counts, as well as other literature data, are well fit by pure luminosity evolution models. Formation redshifts for early type galaxies in excess of $z = 2.5$ are required to fit the ERO counts, and $z \approx 3$ is favoured. However, the range in the colours of EROs suggests also a wide range in formation redshifts.

Acknowledgements. We thank the referee for good and clarifying comments. We are grateful for useful discussion with Kalevi Mattila, Emanuele Daddi, and Margrethe Wold. Emanuele Daddi is especially thanked for providing the ERO count models used in this paper.

References

Bergström, S., & Wiklind, T. 2004, A&A, 414, 95
Bertin, E., & Arnouts, S. 1996, A&AS, 117, 393
Bolzonella, M., Miralles, J.-M., & Pelló, R. 2000, A&A, 363, 476
Bruzual, G., & Charlot, S. 1993, ApJ, 405, 538
Chabrier, G., Baraffe, I., Allard, F., & Hauschildt, P. 2000, ApJ, 542, 464
Cimatti, A., Villani, D., Pozzetti, L., & di Serego Alighieri, S. 2000, MNRAS, 318, 453
Cimatti, A., Daddi, E., Mignoli, M., et al. 2002, A&A, 381, L68
Cimatti, A., Daddi, E., Cassata, P., et al. 2003, A&A, 412, L1
Cohen, M. 1994, AJ, 107, 582
Cole, A., Lacey, C. G., Baugh, C. M., & Frenk, C. S. 2000, MNRAS, 319, 204
Cruz, K. L., Reid, I. N., Liebert, J., Kirkpatrick, J. D., & Lowrance, P. J. 2003, AJ, 126, 2421
Daddi, E., Cimatti, A., Pozzetti, L., et al. 2000a, A&A, 361, 535
Daddi, E., Cimatti, A., & Renzini, L. 2000b, A&A, 362, L45
Daddi, E., Cimatti, A., Broadhurst, T., et al. 2002, A&A, 384, L1
Eggen, O. J., Lynden-Bell, D., & Sandage, A. R. 1962, ApJ, 136, 748
Elbaz, D., & Cesarsky, C. 2003, Science, 300, 270
Firth, A. E., Somerville, R. S., McMahon, R. G., et al. 2002, MNRAS, 332, 617
Fukugita, M., Shimasaku, K., & Ichikawa, T. 1995, PASP, 107, 945
Fukugita, M., Ichikawa, T., Gunn, J. E., et al. 1996, AJ, 111, 1748
Gilbank, D. G., Smail, I., Ivison, R. J., & Packham, C. 2003, MNRAS, submitted [arXiv:astro-ph/0308318]
Gonzalez-Solares, E. A., Perez-Fournon, I., Rowan-Robinson, M., et al. 2004, MNRAS, submitted [arXiv:astro-ph/0402406]
Hall, P. B., & Green, R. F. 1998, ApJ, 507, 558
Irwin, M., & Lewis, J. 2001, NewAR, 45, 105
Kauffmann, G., & Charlot, S. 1998, MNRAS, 297, L23
Kochanek, C. S., Pahre, M. A., Falco, E. E., et al. 2001, ApJ, 560, 566
Landolt, A. U. 1992, AJ, 104, 340
Larson, R. B. 1975, MNRAS, 173, 671
Mann, R. G., Oliver, S., Carballo, R., et al. 2002, MNRAS, 332, 549
Martini, P. 2001, AJ, 121, 2301
Marzke, R. O., Geller, M. J., Huchra, J. P., & Corwin, H. G. 1994, AJ, 108, 437
McMahon, R. G., Walton, N. A., Irwin, M. J., et al. 2001, NewAR, 45, 97
Mohan, N. R., Cimatti, A., & Röttgering, H. J. 2002, A&A, 383, 440
Moriondo, G., Cimatti, A., & Daddi, E. 2000, A&A, 364, 26
Moustakas, L. A., Casertano, S., Conselice, C., et al. 2004, ApJ, 600, L131
Oliver, S., Rowan-Robinson, M., Alexander, D. M., et al. 2000, MNRAS, 316, 749
Pozzetti, L., & Mannucci, F. 2000, MNRAS, 317, L17
Pierini, D., Maraston, C., Bender, R., & Witt, A. N. 2004, MNRAS, 347, 1
Roche, N. D., Almaini, O., Dunlop, J. S., Ivison, R. J., & Willott, C. J. 2002, MNRAS, 337, 1282
Roche, N. D., Dunlop, J. S., & Almaini, O. 2003, MNRAS, 346, 803
Rowan-Robinson, M., Lari, C., Perez-Fournon, I., et al. 2004, MNRAS, in press [arXiv:astro-ph/0308283]
Saracco, P., Longhetti, M., Severgnini, P., et al. 2003, A&A, 398, 127
Scodeggio, M., & Silva, D. R. 2000, A&A, 359, 953
Scott, S. E., Fox, M. J., Dunlop, J. S., et al. 2002, MNRAS, 331, 817
Silva, L., Granato, G. L., Bressan, A., & Danese, L. 1998, ApJ, 509, 103
Silva, L. 1999, Ph.D. Thesis, SISSA (International School for Advanced Studies), Trieste, Italy
Smail, I., Owen, F. N., Morrison, G. E., et al. 2002, ApJ, 581, 844
Smith, G. P., Smail, I., Kneib, J.-P., et al. 2002, MNRAS, 330, 1
Somerville, R. S., & Primack, J. R. 1999, MNRAS, 310, 1087
Takata, T., Kashikawa, N., Nakanishi, K., et al. 2003, PASJ, 55, 789
Totani, T., Yoshii, Y., Maihara, T., Iwamuro, F., & Motohara, K. 2001, ApJ, 559, 592
Väisänen, P., Tollestrup, E. V., Willner, S. P., & Cohen, M. 2000, ApJ, 540, 593 (V00)
Väisänen, P., & Johansson, P. H. 2004, A&A, in press [arXiv:astro-ph/0405056]
White, S. D. M., & Rees, M. J. 1978, MNRAS, 183, 341
White, S. D. M., & Frenk, C. S. 1991, ApJ, 379, 52
Wold, M., Armus, L., Neugebauer, G., Jarrett, T. H., & Lehnert, M. D. 2003, AJ, 126, 1776
Yan, L., & Thompson, D. 2003, ApJ, 586, 765
Yan, L., Thompson, D., & Soifer, B. T. 2003, AJ, 127, 1274